Supporting Information

A Gill-Mimicking Thermoelectric Generator (TEG) for Waste Heat Recovery and Self-Powering Wearable Devices

Yuxiang Zhu,[a] Weiheng Xu,[a] Dharneedar Ravichandran,[a] Sayli Jambhulkar[a] and Kenan Song*[b]

[a] Systems Engineering, The Polytechnic School (TPS), Ira A. Fulton Schools of Engineering, Arizona State University, Mesa, AZ, United States 85212
[b] The Polytechnic School (TPS) & School for Engineering of Matter, Transport and Energy (SEMTE), Ira A. Fulton Schools of Engineering, Arizona State University, Mesa, AZ, United States 85212

*Correspondence author: Kenan.Song@asu.edu

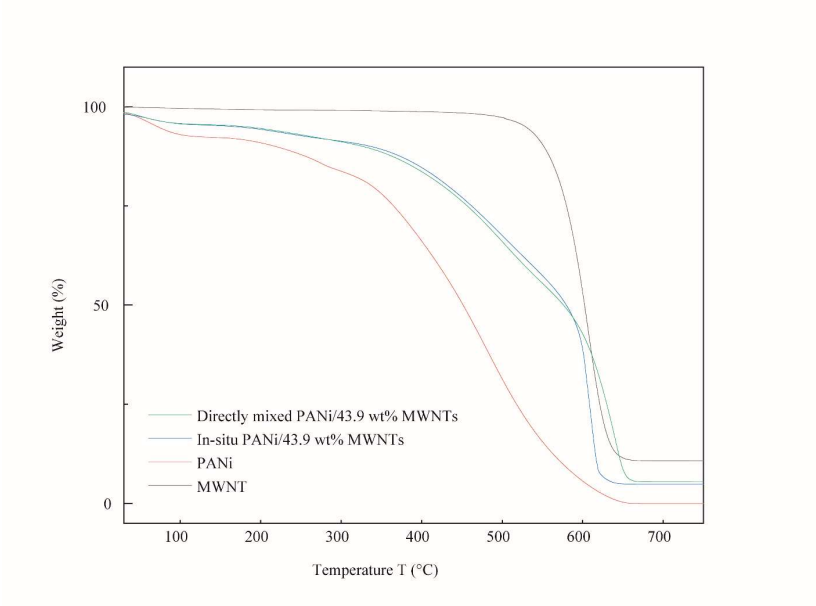

Figure S1. TGA comparison of in-situ polymerized and directly mixed PANi/43.9 wt% MWNTs confirmed the consistency of MWNT concentrations

The conjugated structure endows polyaniline with high thermal stability. The pure PANi experienced a three-step weight loss in air.

(i) The first small step started right above room temperature and stopped at around 110 ^{o}C. This weight drop was due to the moisture captured in the powder.

(ii) The second gentle slope from 200 ^{o}C to 340 ^{o}C corresponds to the loss of counter anion, in our case, the chloride ion.[1]

(iii) At 340 ^{o}C, the slope became steep, and the significant weight loss happened within this range up to 640 ^{o}C. The enormous weight loss corresponds to the decomposition of the PANi backbone, leaving no mass residue.[2]

The in-situ polymerized and directly-mixed PANi/MWNTs with 43.9 wt% of MWNTs were also tested under the same condition. The three-step weight loss was similar to pure PANi below 590 ^{o}C. The MWNT addition improved the thermal stability of PANi, showing higher residue during the thermal sweeping.

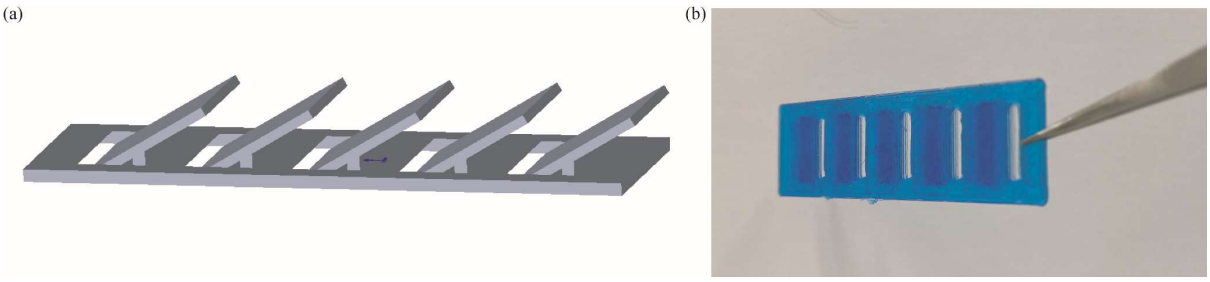

Figure S2. (a) The STL file of the TEG substrate for printing. (b) Photo of the printed substrate bottom. The openings on the bottom of the substrate were to assemble the thermoelectric bulks

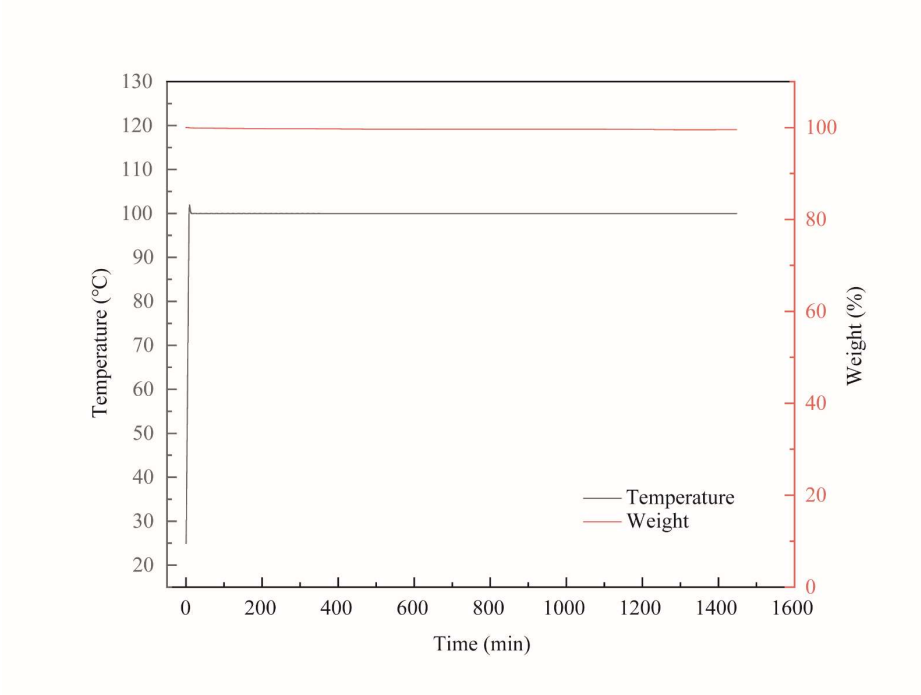

Figure S3. The thermogravimetric analysis (TGA) of the Kapton tape for aging characterizations. The tape's mass loss was negligible at a temperature of 100 °C for 24 h, indicating the thermal stability of the binding material at a working temperature <=100 °C in the vicinity of the surfaces of skins, hot water bottles, and car roofs.

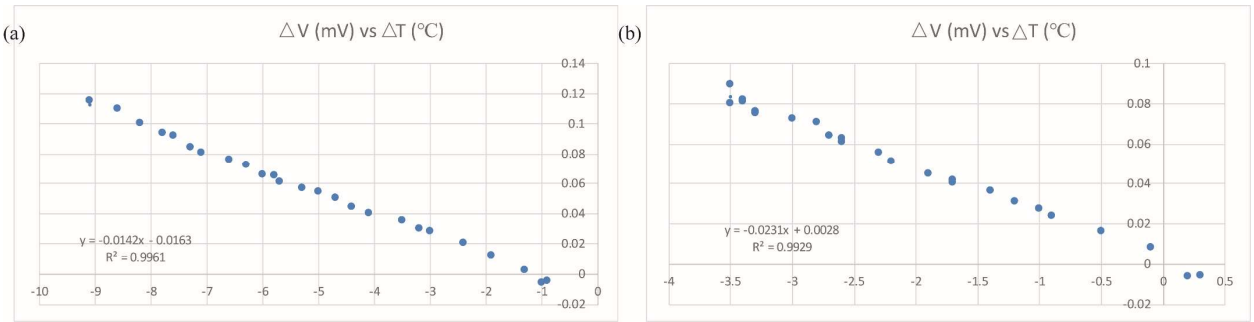

Figure S4. Examples of the linear fitting of the voltage difference (*ΔV*) vs. temperature difference (*ΔT*) to obtain Seebeck coefficient values. (a) In-situ polymerized PANi/28.2 wt% MWNTs, and (b) directly mixed PANi/58.7 wt% MWNTs

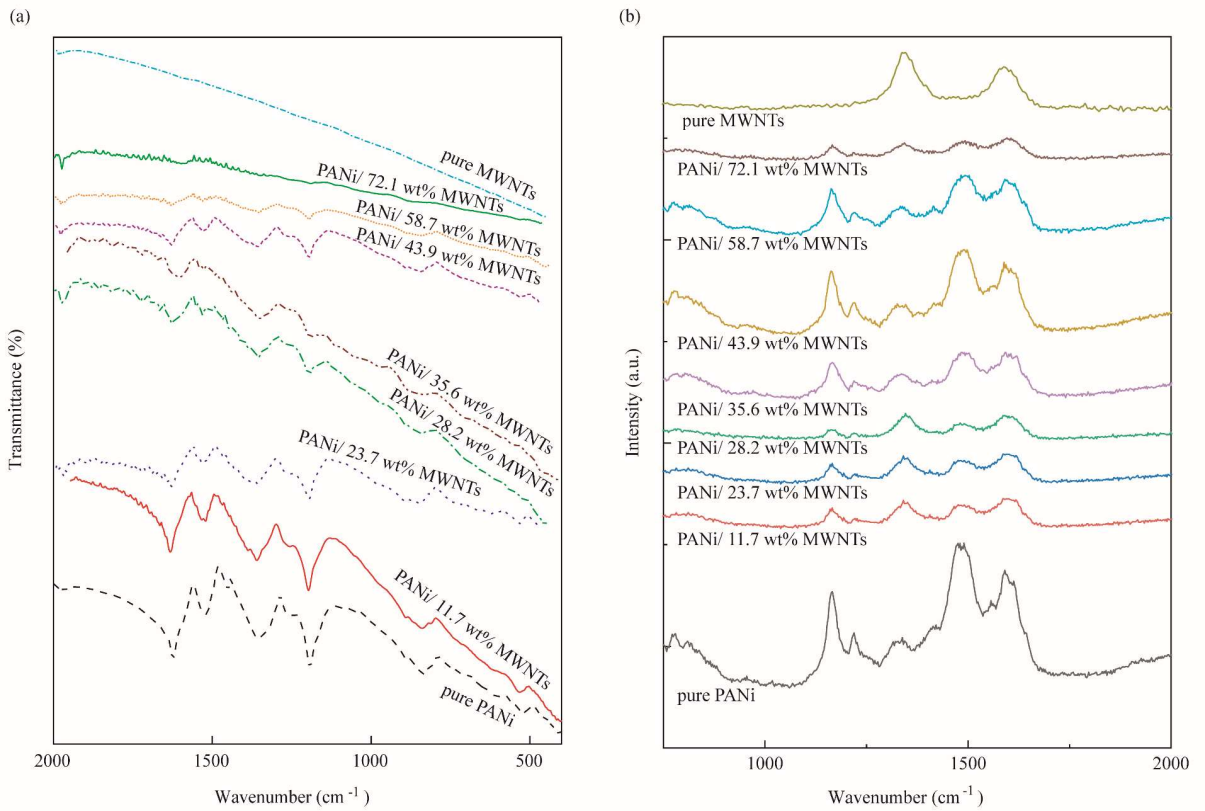

Figure S5. (a) FTIR and (b) Raman spectra for directly mixed pure-PANi, PANi/11.7 wt% MWNTs, PANi/23.7 wt% MWNTs, PANi/28.2 wt% MWNTs, PANi/35.6 wt% MWNTs, PANi/43.9 wt% MWNTs, PANi/58.7 wt% MWNTs, PANi/72.1 wt% MWNTs and pure MWNTs.

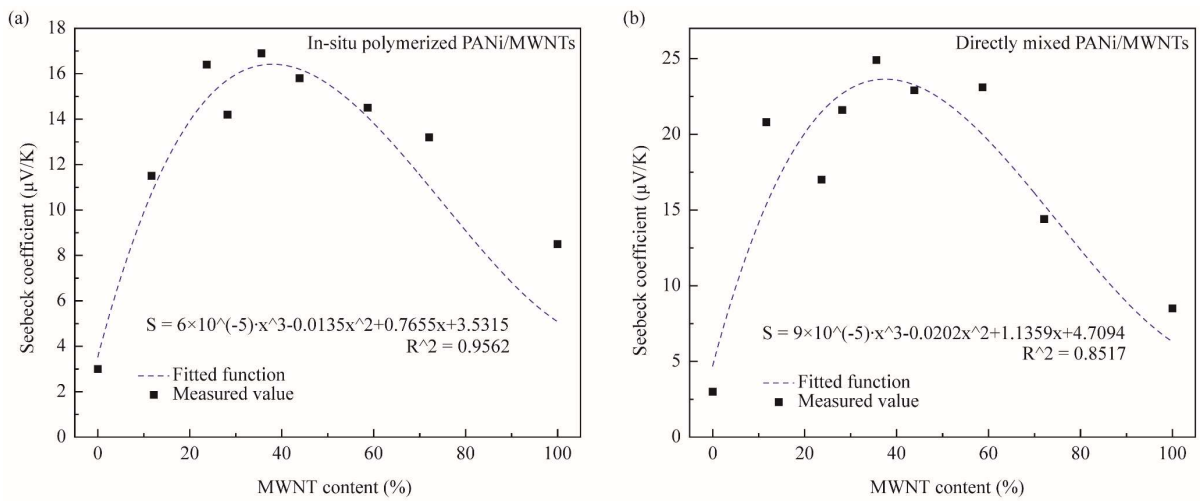

Figure S6. The Seebeck coefficients with different MWNT contents and the polynomial curve fitting of (a) in-situ polymerized PANi/MWNTs and (b) directly mixed PANi/MWNTs

The Seebeck coefficients from the in-situ polymerized and directly-mixed samples were fitted with a cubic function ($S = 6 \times 10^{-5} \cdot x^3 - 0.0135x^2 + 0.7655x + 3.5315$ for in-situ PANi/MWNTs and $S = 9 \times 10^{-5} \cdot x^3 - 0.0202x^2 + 1.1359x + 4.7094$ for directly mixed PANi/MWNTs, respectively). The Seebeck coefficient's rapid increase at low MWNT content was due to the MWNT phase and their comparatively uniform dispersions. The interphase between the PANi/MWNT phases induced the energy filtering effect, enhancing the Seebeck coefficient.[3,4] With higher MWNTs content, the carrier concentration rises. According to $S = \frac{8\pi^2\kappa_B^2}{3eh^2} m^* T (\frac{\pi}{3n})^{2/3}$,[5,6] the deterioration of the coefficient dominated when MWNTs content is higher than 40%, in addition to the worse dispersion and widely distributed voids and defects, resulting in the overall drop of the Seebeck coefficient.

Table S1. Mechanical properties of cold-pressed pure PANi, pure MWNTs, in-situ polymerized and directly mixed PANi/MWNTs composite bulks

Sample	Tensile strength (MPa)	Young's modulus (GPa)	Tensile Strain (%)
Pure PANi	2.028 ± 0.3005	0.4651 ± 0.1607	0.8302 ± 0.3956
In-situ PANi/11.7 wt% MWNTs	2.122 ± 0.5496	0.9701 ± 0.2028	0.4860 ± 0.2176
In-situ PANi/23.7 wt% MWNTs	3.428 ± 0.7026	0.9896 ± 0.2787	0.5916 ± 0.1486
In-situ PANi/28.2 wt% MWNTs	4.022 ± 0.9793	1.134 ± 0.2087	0.5864 ± 0.1729
In-situ PANi/35.6 wt% MWNTs	4.432 ± 0.9275	1.434 ± 0.3190	0.4899 ± 0.0688
In-situ PANi/43.9 wt% MWNTs	6.540 ± 0.5350	1.127 ± 0.2487	0.8391 ± 0.1933
In-situ PANi/58.7 wt% MWNTs	11.470 ± 1.6770	2.017 ± 0.1843	1.0898 ± 0.2205
In-situ PANi/72.1 wt% MWNTs	5.586 ± 0.6222	0.9961 ± 0.2772	0.8055 ± 0.1675
Directly mixed PANi/11.7 wt% MWNTs	3.075 ± 0.2287	0.8399 ± 0.1697	0.5630 ± 0.1318
Directly mixed PANi/23.7 wt% MWNTs	2.774 ± 1.0420	0.8287 ± 0.1287	0.5177 ± 0.1654
Directly mixed PANi/28.2 wt% MWNTs	1.216 ± 0.2998	0.6003 ± 0.1667	0.4231 ± 0.1125
Directly mixed PANi/35.6 wt% MWNTs	1.446 ± 0.5200	0.4703 ± 0.2978	0.6260 ± 0.3319
Directly mixed PANi/43.9 wt% MWNTs	1.553 ± 0.3282	0.3606 ± 0.0587	0.7492 ± 0.0814
Directly mixed PANi/58.7 wt% MWNTs	1.423 ± 0.5633	0.4118 ± 0.0914	0.7040 ± 0.3519
Directly mixed PANi/72.1 wt% MWNTs	0.6568 ± 0.3049	0.1661 ± 0.0769	0.8661 ± 0.4651
Pure MWNTs	0.8910 ± 0.1853	0.1405 ± 0.0349	1.274 ± 0.3806

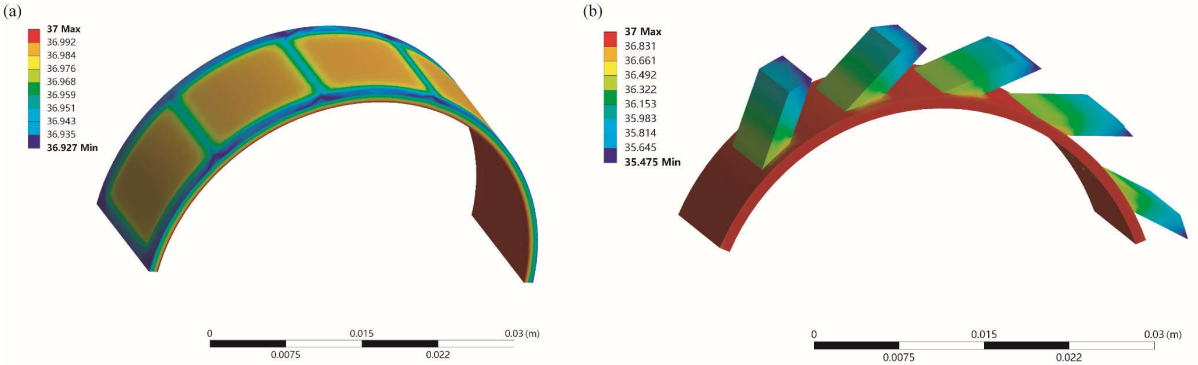

Figure S7. The simulated temperature distribution of (a) the in-plane design TEG and (b) the out-of-plane, gill-mimicking TEG at a curving state with a bending displacement of 2 cm. The maximum temperature difference of the flat design TEG is below 0.1 ^{o}C, while the gill-mimicking TEG can obtain a temperature difference of ~1.5 ^{o}C, showing the same consistent trend of the thermal mapping between the curving and flat substrates.

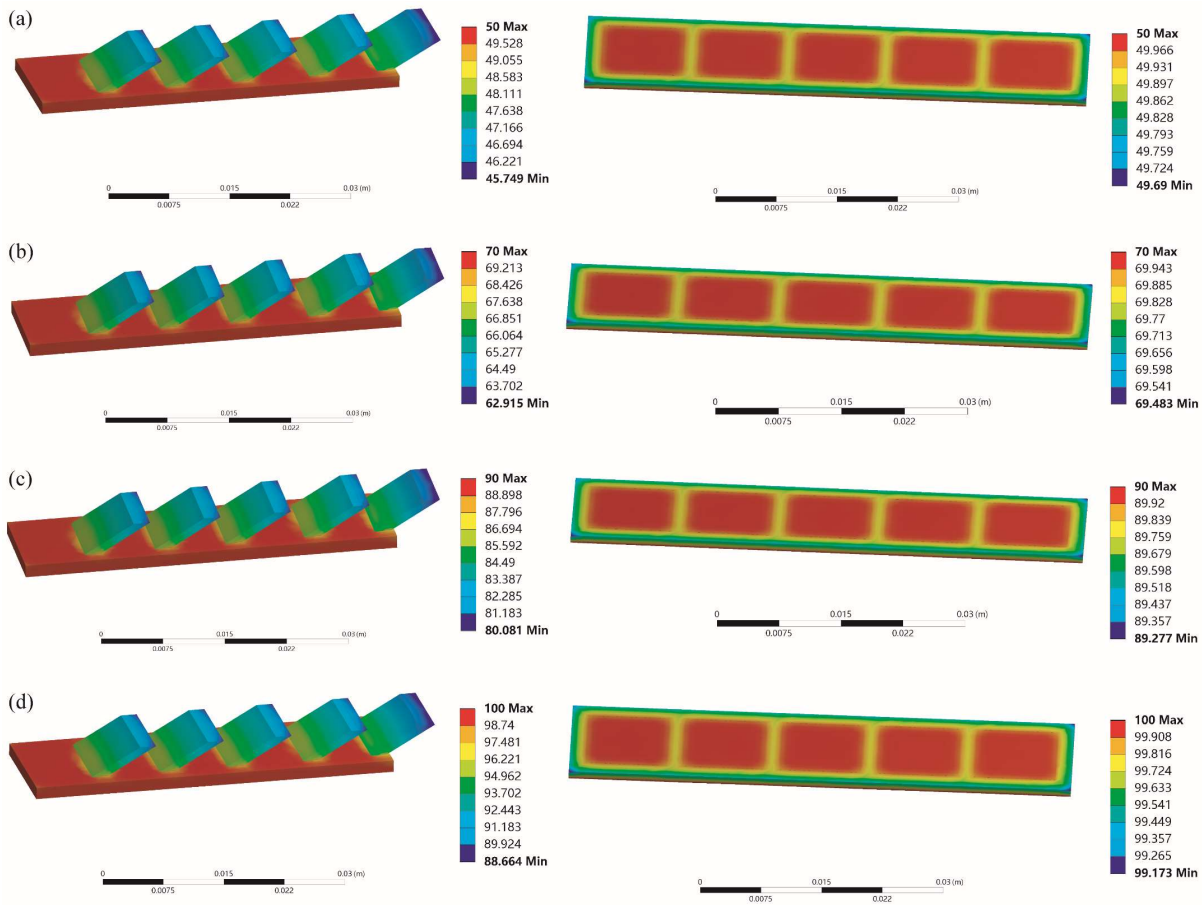

Figure S8. The Finite Element Method (FEM) simulation of a gill-inspired design of fTEG (left) and a flat design of TEG (right) with the substrate (hot side) temperature of (a) 50 ^{o}C, (b) 70 ^{o}C, (c) 90 ^{o}C, and 100 ^{o}C.

Table S2. TE property of polymer/carbon-based composites in literature as compared with our work

Material	Processing method	Power factor (μW m^{-1} K^{-2})	Generator assembled	Organic solvent	Manufacturing time (h)	Flexibility for wearability	Out-of-plane design	Year
PANi/MWNTs	*in-situ* polymerization, cold pressing	1.254	Yes	No	~20	Yes	Yes	This work
PANi/PbTe	*in-situ* polymerization, cold pressing	0.8	No	Yes	>24			2011[7]
PANi/Graphite	Mechanical mixing, cold pressing	4	No	No	~30			2011[8]
PANi/CNT	*in-situ* polymerization, electro-spinning	0.17	No	Yes	~47			2012[9]
PANi/GNPs	Cold pressing	14	No	No	~60			2013[10]
PANi/GNPs	Solution dispersion, drop-casting	19	No	Yes	~60			2014[11]
PEDOT:PSS/Ionic liquid/PU	Drop casting	~4.8	Yes	No	~21	Yes	No	2020[12]
PEDOT:PSS & n-type CNT	Gelation process	4.77	Yes	Yes	>48	Yes	No	2018[13]
Polypyrrole/Silver	One pot photo-polymerization	0.03	Yes	Yes	>1.5	Yes	No	2017[14]
PEDOT:PSS/BiSbTe	Drop casting	8.3	Yes	Yes	>24	Yes	No	2019[15]
PbTe-modified PEDOT	Interfacial polymerization	1.45	No	Yes	>24			2011[16]
PEDOT/SWCNT	Direct mixing	25	No	Yes	>144			2010[17]

Polythiophenes	Solution casting	~10	No	Yes	~12			2015[18]
FBDPPV	Chemical synthesis	~7	No	Yes	Varies with different dopants			2019[19]
Bacteria nanocellulose/CNT	Bacteria culture	~30	Yes	Yes	>295, including inoculum culture	Yes	No	2019[20]
Carbonized polydopamine	Coating, heat treatment	0.2	No	No	~60			2017[21]
Polypyrrole/rGO	Soft template polymerization	8.57	No	No	~36			2015[22]
PVA/Bi_2Te_3	Solid-state reaction, screen printing	0.04	Yes	No	>38, excluding solid-state reaction	Yes	No	2019[23]
P3HT-TFSI	Drop-casting	~24	No	Yes	>3, depends on doping time			2012[24]
P3HT-F_4TCNQ	Vapor doping, spin casting	27	No	Yes	~1, varies with dopant amount			2018[25]
Polypyrrole	Chemical oxidative polymerization	~24	No	Yes	>32, depends on oxidation time			2017[26]
Polypyrrole/PANi/SWCNT	*in-situ* polymerization	19.2	No	Yes	~48			2020[27]

With easy availability and facile processing, current organic TE materials find it hard to compete with traditional inorganic alloys or their composites in the figure of merit or power factor (**Table S2**). However, the high power factor has usually been mostly achieved by sacrificing device density, flexibility, or assembly simplicity. For example, Yuan et al. were able to obtain a power of 190 μW with the body temperature by using p-type and n-type semiconductors attached to metals/conductive polymers.[28] With the extremely high number of 576 pieces of TE grains, which is over 100 times more than ours, they still need a boost converter to raise the voltage to 2-3 V by sacrificing some power to be compatible with an LCD screen and other sensors. Put simply, our current TEG can work with a strain switch to reveal joint movements and respiration cycles. To further include multiple sensors, such as gyro sensors and humidity sensors, or improve user-friendliness by introducing an electronic display, we can increase the output power and voltage by simply increasing the number of gills in the TEG device. Our gill-mimicking structure can also enhance the thermoelectric performance via the following protocols. (i) Exploring the n-type TE bulks to match the current p-type PANi/MWNTs. Most conducting polymers are p-type, with positive charge holes as the primary carriers. A complete TE pair will improve energy efficiency. (ii) Using inorganic semiconductors with our MWNTs as hybrid materials but sacrificing a larger density and more expensive raw materials.

References

1 N. Chandrakanthi and M. A. Careem, *Polym. Bull.*, 2000, **44**, 101–108.
2 L. Ding, X. Wang and R. V. Gregory, *Synth. Met.*, 1999, **104**, 73–78.
3 W. Park, H. Hwang, S. Kim, S. Park and K. Jang, *ACS Appl. Mater. Interfaces*, 2021, **13**, 7208-7215.
4 Y. Wang, C. Yu, M. Sheng, S. Song and Y. Deng, *Adv. Mater. Interfaces*, 2018, **5**, 7–9.
5 Y. Du, J. Xu, B. Paul and P. Eklund, *Appl. Mater. Today*, 2018, **12**, 366–388.
6 Y. Wang, L. Yang, X. Shi, X. Shi, L. Chen, M. S. Dargusch, J. Zou and Z. Chen, *Adv. Mater.*, 2019, **31**, 1807916.
7 Y. Y. Wang, K. F. Cai, J. L. Yin, B. J. An, Y. Du and X. Yao, *J. Nanoparticle Res.*, 2011, **13**, 533–539.
8 L. Wang, D. Wang, G. Zhu, J. Li and F. Pan, *Mater. Lett.*, 2011, **65**, 1086–1088.
9 Q. Wang, Q. Yao, J. Chang and L. Chen, *J. Mater. Chem.*, 2012, **22**, 17612–17618.
10 B. Abad, I. Alda, P. Díaz-Chao, H. Kawakami, A. Almarza, D. Amantia, D. Gutierrez, L. Aubouy and M. Martín-González, *J. Mater. Chem. A*, 2013, **1**, 10450–10457.
11 L. Wang, Q. Yao, H. Bi, F. Huang, Q. Wang and L. Chen, *J. Mater. Chem. A*, 2014, **2**, 11107–11113.
12 N. Kim, S. Lienemann, I. Petsagkourakis, D. Alemu Mengistie, S. Kee, T. Ederth, V. Gueskine, P. Leclère, R. Lazzaroni, X. Crispin and K. Tybrandt, *Nat. Commun.*, 2020, **11**, 1-10.
13 J. Liu, Y. Jia, Q. Jiang, F. Jiang, C. Li, X. Wang, P. Liu, P. Liu, F. Hu, Y. Du and J. Xu, *ACS Appl. Mater. Interfaces*, 2018, **10**, 44033–44040.
14 M. Bharti, A. Singh, S. Samanta, A. K. Debnath, D. K. Aswal, K. P. Muthe and S. C. Gadkari, *Energy Convers. Manag.*, 2017, **144**, 143–152.
15 M. Bharti, A. Singh, G. Saini, S. Saha, A. Bohra, Y. Kaneko, A. K. Debnath, K. P. Muthe, K. Marumoto, D. K. Aswal and S. C. Gadkari, *J. Power Sources*, 2019, **435**, 226758.
16 Y. Wang, K. Cai and X. Yao, *ACS Appl. Mater. Interfaces*, 2011, **3**, 1163–1166.
17 D. Kim, Y. Kim, K. Choi, J. C. Grunlan and C. Yu, *ACS Nano*, 2010, **4**, 513–523.
18 A. M. Glaudell, J. E. Cochran, S. N. Patel and M. L. Chabinyc, *Adv. Energy Mater.*, 2015, **5**, 1–8.
19 H. Un, S. A. Gregory, S. K. Mohapatra, M. Xiong, E. Longhi, Y. Lu, S. Rigin, S. Jhulki, C. Yang and T. V Timofeeva, *Adv. Energy Mater.*, 2019, **9**, 1900817.
20 D. Abol-Fotouh, B. Dörling, O. Zapata-Arteaga, X. Rodríguez-Martínez, A. Gómez, J. S. Reparaz, A. Laromaine, A. Roig and M. Campoy-Quiles, *Energy Environ. Sci.*, 2019, **12**, 716–726.
21 H. Li, Y. V. Aulin, L. Frazer, E. Borguet, R. Kakodkar, J. Feser, Y. Chen, K. An, D. A. Dikin and F. Ren, *ACS Appl. Mater. Interfaces*, 2017, **9**, 6655–6660.
22 Z. Zhang, G. Chen, H. Wang and W. Zhai, *J. Mater. Chem. C*, 2015, **3**, 1649–1654.
23 A. L. Pires, I. F. Cruz, J. Silva, G. N. P. Oliveira, S. Ferreira-Teixeira, A. M. L. Lopes, J. P. Araújo, J. Fonseca, C. Pereira and A. M. Pereira, *ACS Appl. Mater. Interfaces*, 2019, **11**, 8969–8981.
24 Q. Zhang, Y. Sun, W. Xu and D. Zhu, *Energy Environ. Sci.*, 2012, **5**, 9639–9644.
25 E. Lim, K. A. Peterson, G. M. Su and M. L. Chabinyc, *Chem. Mater.*, 2018, **30**, 998–1010.
26 L. Liang, G. Chen and C. Y. Guo, *Mater. Chem. Front.*, 2017, **1**, 380–386.
27 S. Wang, Y. Zhou, Y. Liu, L. Wang and C. Gao, *J. Mater. Chem. C*, 2020, **8**, 528–535.
28 J. Yuan, R. Zhu and G. Li, *Adv. Mater. Technol.*, 2020, **5**, 1–7.